Band 41 (2007), S. 55–75

ZEITSCHRIFT FÜR
GLETSCHERKUNDE
UND GLAZIALGEOLOGIE

Semi-automatic glacier delineation from Landsat imagery over Hintereisferner in the Austrian Alps

JOHAN P. M. HENDRIKS AND PETRI PELLIKKA, HELSINKI

With 7 figures

Abstract

In this study a procedure is presented to semi-automatically derive glacier delineations from Landsat satellite imagery for Hintereisferner, a glacier in the Austrian Alps. Spectral information inherent to imagery was utilised to derive the masks and existing manual glacier outlines from maps served as reference data for validation of masks for the years 1991 and 1997. Within the first step of the model a water mask is created. It requires as input the raw satellite image and an upper range of 20–30% of Digital Number value counts in the histogram of the Normalised Difference Water Index. The second step, which creates the glacier mask, requires as input the raw satellite image and the water mask. It uses a threshold value for (E)TM(+)5 to mask clouds and assumes saturated pixels to be glacier if not identified as clouds. Finally it automatically calculates a Normalised Difference Snow Index threshold value of 0.5–0.7 based on the variable range in Digital Number values for each image. After performing accuracy analyses omissions ±17% and ±13% for the years 1991 and 1997 were found. The omissions were located at the margins of the glacier where debris on the surface prohibited a spectral differentiation between glacier and nearby slopes. A change analysis for the period 1991–1997 revealed an omission of 16% in unchanged area for the surface of Hintereisferner. The area of Hintereisferner was determined within a range of –10.8% and +8.7% when compared to conventional photogrammetric measurements. In the period 1985–1999 the area of Hintereisferner and its neighbouring glaciers decreased from 159 km^2 to 138 km^2. During the reference period 1991–1997 the decrease was 6 km^2.

Halbautomatische Abgrenzung der Gletscherfläche des Hintereisferners von Landsat-Bildern

Zusammenfassung

In dieser Arbeit wird ein halbautomatisches Verfahren vorgestellt, mit dem aus Landsat-Bildern die Umrisse des Hintereisferners und seiner Nachbarn in den Ötztaler Alpen bestimmt wurden. Aus der spektralen Information der Bilder wurden Masken abgeleitet, die vorhandene manuelle Auswertung aus Landkarten der Jahre 1991 und 1997 diente zur Validierung der Satellitenauswertung. Zuerst wurde aus den rohen Satellitenbildern und dem Histogramm des *Normalized Difference Water Index* eine Maske für Wasserflächen gebildet. In einem zweiten Schritt wurde eine Gletschermaske hergestellt, wozu die Wassermaske und wieder die rohen Satellitenbilder verwendet wurden. Die Gletschermaske braucht einen Schwellwert für (E)TM(+)5, um Wolken auszuscheiden und interpretiert außerhalb der Wolken gesättigt Pixel als Gletscherfläche. Schließlich wird automatisch ein Schwellwert für den *Normalized Difference Snow Index* berechnet. Bei der Analyse der Verlässlichkeit der Ergebnisse wurden für 1991 17% und für 1997 13% Fehlbetrag festgestellt. Die Fehler lagen an den Gletscherrändern, wo Schuttbedeckung des Eises die spektrale Unterscheidung von Gletschern und eisfreien Bereichen nicht zuließ. Im Vergleich zu konventionellen, photogrammetrischen Werten ergab die Bestimmung der Flächenänderung des Hintereisferners einen Fehlbetrag von 16%. Das gesamte Untersuchungsgebiet hatte von 1985 bis 1999 eine reale Flächenabnahme von 159 auf 138 km^2.

1. Introduction

Glaciers in the Alps have been monitored and mapped extensively since the end of the Little Ice Age around 1850 (Kuhn et al. 1997). Recurrent photography and written documents based on extensive and laborious field campaigns have led to the publication of the first topographic maps at the end of the 19th century (Blümcke and Hess 1899). In some cases climatic records go back further in time. They support the observations on the loss of mass of most glaciers in the Alps as a result of regional climatic change. Accurate topographic maps, showing the glaciers' extents have been produced irregularly at times and normally have intervals that span decades (Paul et al. 2004).

One of the most intensively and repeatedly surveyed glaciers in Austria, Hintereisferner (Fig. 1) is situated at 10°46'E, 46°48'N at the southwest end of the valley Ventertal, a NE-SW running side valley of the Ötztal that ends at the Italian border. Hintereisferner has the typical geometry of a valley glacier, ranges in elevation between 2500–3700 m asl., in 2003 covered an area close to 8 km^2 and had a length of 7 km.

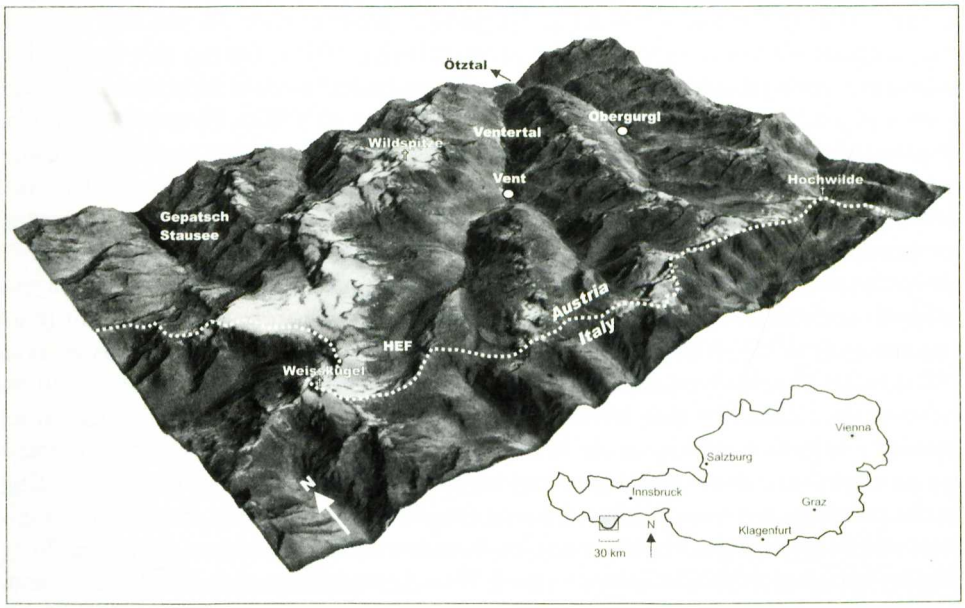

Figure 1. Slant view towards NE of the region of Hintereisferner (HEF) in the Austrian Alps. The view consists of a Landsat TM image (1999) in band combination 5/4/3 that was resolution-merged with its panchromatic band and draped over a 30-m DEM.

The first map of Hintereisferner that was published in 1894, historical documents, dendrochronology and geomorphological studies go farther back in time. Surveys on the motion of Hintereisferner started in 1894 (Blümcke & Hess 1899). The specific mass balance of Hintereisferner using the direct glaciological method has been calculated since 1953 (Hoinkes 1970, Span 1993). Since the glacier's maximum extent in 1850 it has been continuously retreating except for the 60 m advance in the period 1918–1922 (Span et al. 1997). It experienced accelerated flow events in 1920, 1943 and 1978 (Kuhn et al. 1996). The annual specific mass balance of Hintereisferner has been positive for only 10 times between the glaciological years 1953 and 1997 (Kuhn et al. 1999).

Since the launch of the first Landsat satellite in 1972, periodic observation of a particular place on Earth entered a new era as it became significantly easier to perform multi-temporal analyses. The Landsat programme has continued to evolve. The ETM+ (Enhanced Thematic Mapper) aboard the Landsat 7 satellite was launched in 1999 and produces imagery with a spatial resolution in its panchromatic band that is more than 5 times better when compared to bands 1–4 of the MSS (Multi-Spectral Scanner) sensor on Landsat 1. The panchromatic band of the ETM+ has a spatial resolution of 15 metres compared to a spatial resolution of 80 metres of bands 1–4 of the MSS sensor. Spectral ranges and resolutions have improved considerably during this period

as well. During the mid–1970's Landsat images were utilised for the first time in glaciological studies to detect glacier zones (Østrem 1975). During this time, false colour and contrast enhanced MSS composites served as tools to identify ice boundaries and glacier extent (Rott 1976, Della Ventura et al. 1983). Manual delineation of glacier boundaries on Landsat images by experts showed better results than automated methods, but seemed too laborious for individual glaciers (Rott and Markl 1989). More recently, different approaches for thresholding and segmenting ratio images derived from TM (Thematic Mapper) or ETM+ bands have been used. In most cases classification procedures, additional GIS (Geographical Information Systems) methods and band combinations were exercised to produce an accurate result (e.g. Gratton et al. 1990, Kääb et al. 2002). Even after accurate transformations of raw DN (Digital Number) values into surface reflectances, practically all of the studies came to the conclusion that ice tongues and boundaries mantled with debris cause problems (e.g. Koelemeijer et al. 1993). Attempts to delineate ice-moraine contacts are precluded as debris-covered ice and moraines cannot be discriminated spectrally in the visible to shortwave infrared bands (Paul 2002). Heiskanen et al. (2003) successfully delineated glacier borders in cast shadows in the Svartisen ice cap in Norway by applying threshold values to the ETM+ thermal infrared band. Hendriks and Pellikka (2004) experimented with a glacier masking procedure combining a thresholded NDSI (Normalised Difference Snow Index) image and the thermal band of ETM+. Disturbances like clouds and shadows were removed but some areas were misrepresented due to striping in the thermal band. Paul (2000) made a clear evaluation of different methods for glacier mapping using TM data. After comparison of a TM derived outline to a manually created outline on a SPOT Pan scene he concluded that segmenting a ratio image from TM4 / TM5 containing raw DNs results in the best glacier mask. Bayr et al. (1994) had already earlier delineated the ablation zone of two glaciers using this method. Recently Silverio and Jaquet (2005) mapped glacial areas in Peru by applying separate NDSI thresholding values to spectrally separate glaciers and debris-covered glaciers.

The objective of this study is to develop a two-step interactive modelling procedure to create glacier masks from Landsat (E)TM(+) images containing only raw DN values. A masking procedure would normally refer to obscure glacier areas, but instead the term is used here to identify the glacier area. The glacier masking procedure should be accurate and fed only by spectral bands. A minimum amount of assumptions, thresholds and manual alterations is desired. The procedure chosen here is based on the NDSI thresholding method improving the result by semi-automatically filtering clouds, saturated pixels and water areas. The accuracy of the masks is validated against existing digital grids that were derived from manual delineations. The masks are also compared to NDSI masks in order to see the improvement of the modelling process from standard method (Hall et al. 1995b). The model should not require multiple additional datasets such as a GIS or supplementary correction procedures in different software packages

2. Data

In total seven orthorectified Landsat images were analysed. All images have a radiometric resolution of eight bits, which means a DN values range of 0–255. The oldest image dates from 1985 and the latest one was acquired in 2002. Those images were selected that had acquisition dates within two months from the turnover of the mass balance year (Mass balances for glaciers are normally computed for the period 1st Oct.–30th Sept.). Table 1 presents the date of the imagery and the respective solar azimuth and solar elevation angles. For glaciological purposes the low elevation angles in the rough terrain create cast shadows on the glacier surface hampering the analysis (Heiskanen 2003). The Landsat 4–5 and 7 missions have a sun synchronous orbit, produce imagery 185 km wide on a side and have a repeat coverage of 16 days. Landsat satellites use the Worldwide Reference System (WRS) of scenes divided up into paths and rows. Each scene of the TM sensor has seven distinct bands covering the visible to the thermal-infrared part of the spectrum. These bands comprise a spectral range of 0.45–12.50 µm; the thermal-infrared band has a spatial ground resolution of 120 m, all the other bands have a 30-m ground resolution. Scenes of the ETM+ sensor contain eight bands covering the same spectral range as the TM sensor; the spatial resolution ranges from 60 m in the thermal band to 15 m in its single panchromatic band. All the other bands have a 30-m ground resolution. More specifications of the different Landsat missions can be found at http://landsat.gsfc.nasa.gov/project/Comparison.html.

Table 1. Overview of the Landsat data (TM or ETM+) and grids derived from manual delineations. The years for manual delineations refer to the "Gletscherstand" (glacier position) in that particular year, not to the publication year of the map. The different steps in processing history apply to all of the manual delineations of maps between 1894 and 1979.

Landsat data					
Date	**Sensor**	**Mission**	**Path/row**	**Solar azimuth (°)**	**Solar elevation (°)**
30.09.1985	TM	Landsat 4	193/27	151	36
03.10.1986	TM	Landsat 4	193/27	149	34
03.08.1990	TM	Landsat 4	193/27	134	53
30.08.1991	TM	Landsat 5	193/27	140	45
15.09.1997	TM	Landsat 5	193/27	148	41
13.09.1999	ETM+	Landsat 7	193/27	154	44
20.08.2002	ETM+	Landsat 7	193/27	145	51

Manual delineations	
Year	**Processing history**
1894, 1920, 1939, 1953, 1964, 1967, 1969, 1979	DEMs derived from historical maps for these years. Maps were digitised and a 15-m grid calculated. Interpolation: Standard Kriging. Reference system: Austrian national coordinate system
1991 1997	DEMs from photogrammetric contour plans (1991) or the Austrian Glacier Inventory (1997). Maps were digitised and a 15-m grid calculated. Interpolation: Standard Kriging. Reference system: Austrian national coordinate system

The oldest historical map showing the position of Hintereisferner and surroundings of present day standard is from 1894 (Blümcke and Hess 1899) and the newest one from 1979 (Schlosser 1996). Although the Austrian Alpine Club frequently publishes new updated maps, less often the glacier position is updated (Hall et al. 2003). The historical maps of Hintereisferner were converted into digital maps at the Institute of Meteorology and Geophysics, University of Innsbruck. In addition to historical maps, contour plans, the aerial photography acquired during 1996–1999 for the compilation of the Austrian Glacier Inventory were analysed, digitised and put into a GIS (Würländer and Kuhn 2000, Lambrecht and Kuhn 2007). The contour lines were interpolated into grids (GeoTIFF format, UTM zone 32) using the Standard Kriging interpolation method and have a resolution of 15 m. Grids contain elevation values derived from isolines on maps (Table 1).

3. Methodology

3.1 Pre-processing of datasets

Before the different datasets could be taken into use, a few pre-processing steps had to be made. The DEMs of Hintereisferner were converted into Boolean maps showing either glacier or non-glacier areas. The grids were imported into the professional remote sensing software Erdas Imagine© where all the spatial and spectral analyses were carried out. To make the grids comparable to the satellite data, their resolution was changed from 15 m to 30 m to conform with the spatial ground resolution of the (E)TM(+) sensor. Depending on the quality of source data, some computed grids were supplied both with and without the dead-ice body at the snout. In these cases the grids without the dead-ice were used, as margins of the glacier may be covered with debris

and cannot be distinguished spectrally from scree on slopes (Koelemeijer et al. 1993). For Hintereisferner these grids were considered as the most accurate reference data available to compute the accuracy of the glacier masking procedure.

No radiometric or atmospheric corrections were carried out for the satellite imagery since the aim was to develop such a method in which they were not compulsory. A subset was defined for Hintereisferner and its neighbouring glaciers. The upper-left and lower-right UTM coordinates that define the rectangular bounding box are 627360,5202720 (UL x,y) and 662490,5177550 (LR x,y). Furthermore, a subset had to be defined for the individual area of Hintereisferner (Figure 2). This was done to allow the most accurate comparison between the reference grids and the generated glacier masks. All grids were tested on the presence of glacier pixels. Any glacier pixels present in either of the grids between 1894 and 1997 were added to the subset.

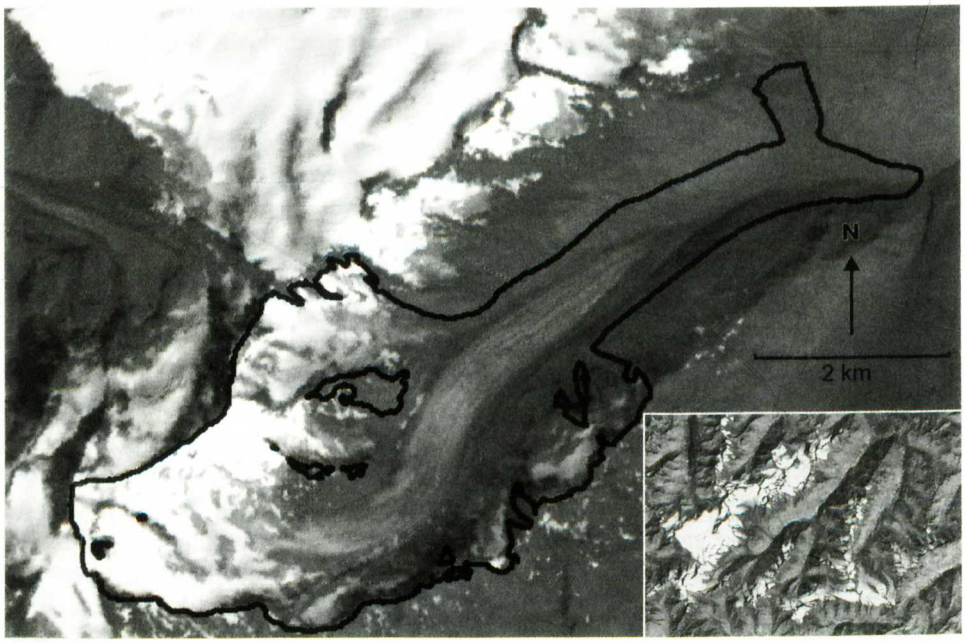

Figure 2. Definition of the subset boundary for Hintereisferner only. The background is a false colour composite Landsat ETM+ image from 1997 displayed in grey scale. The inset presents the analysed area of both Hintereisferner and its neighbouring glaciers used for analysis. The black line in the main image is the outline of the grid derived from the manual delineations performed in the Austrian Glacier Inventory.

3.2 Glacier masking

The masking procedure consists of two steps. The first step encompasses the treatment of water areas in a Landsat (E)TM(+) image. McFeeters (1996) introduced the NDWI (Normalised Difference Water Index) that discriminates water features in a multispectral image. The index is calculated as follows:

$$NDWI = [Green - NIR] / [Green + NIR] \quad (1)$$

The green and near-infrared (NIR) bands needed to calculate the NDWI correspond to (E)TM(+) bands 2 and 4 respectively. The results of the index can range from –1 to +1 where water areas have positive values. It was concluded that this rule does not apply to images containing both glaciers and water. After investigation of the created NDWI images the upper 20–30 % of the range in DN value counts in each image was designated as water. The water masks were calculated as follows:

$$[DN_{max} - [DN_{max} - DN_{min}] \times threshold] / 100 \quad (2)$$

where DN_{max} is the maximum DN value and DN_{min} the minimum DN value in the NDWI image. The threshold value may vary per image and normally lies between 20 and 30 %. The threshold value is determined by visual inspection of the resulting NDWI image and comparison to the available digitized topographic maps.

The creation of the water mask was not very sensitive to small variations (e.g. 1 %) in the threshold as a sieving operator was built into the model that removed interconnected clumps smaller than 10 pixels. A good water mask that forms an exact overlap with digitized topographic maps showing water areas was acquired after 2–3 model runs.

The second part of the model creates the glacier mask (Figure 3). It uses the NDSI, saturated pixels, the water mask and (E)TM(+) band 5 within a set of conditional operators. The NDSI is often used for discrimination between snow, soil, rocks and cloud cover (Silverio and Jaquet 2005). Besides the ability to map snow in rough topography (Sidjak and Wheate 1999) this index provides a good contrast between bare ice and its surroundings at the glacier tongue (Hall et al. 2003). The index is calculated from DN values (Hall et al. 1995b):

$$NDSI = [TM2 - TM5] / [TM2 + TM5] \quad (3)$$

Whenever the NDSI is calculated, the threshold is found by visually inspecting the image and sampling NDSI values. Typical NDSI values for Landsat images lie between 0.5–0.7 and are different for almost any image due to illumination differences. This is not very practical whenever dealing with a large set of images in monitoring studies. Therefore a looping operation was implemented. Hall et al. (1988) pointed out that the

sensor saturation is a major problem over glaciated areas. This inconvenient tendency of the sensor was utilised to recalculate the NDSI value. The NDSI threshold was initially set to 0.5. Thereafter the model simultaneously calculated an initial NDSI mask and a saturation mask from (E)TM(+)1. The saturation mask contained Boolean values with a DN value of 254 and 255. Having the NDSI threshold set very low, it was assumed that the amount of Boolean values in the initial NDSI mask was higher than in the saturation mask. Thereafter the following equation was solved to obtain a new threshold value:

$$NDSI_{threshold} = 0.5 + [[SUM_{saturated} / SUM_{NDSI\ 0.5}] \times 0.2] \quad (4)$$

where $SUM_{saturated}$ is the sum of saturated pixels in (E)TM(+)1, $SUM_{NDSI-0.5}$ is the sum of pixels in the NDSI mask with threshold value 0.5. The value 0.2 refers to the typical range in NSDI values for Landsat images. Equation 4 does not have a physical meaning but is able to recalculate a threshold value based on the range between saturated and initial NDSI pixels. Apparently there is a relationship between the amount of saturation (caused by solar illumination angle and slope orientation) and distribution of the NDSI histogram.

Band 5 of the (E)TM(+) sensor is frequently used for cloud cover detection (Choi and Bindschadler 2004). The model here uses band 5 to remove potential clouds from an image. Masks were calculated using DN $\leq$ 40. As clouds are highly reflective (van Leeuwen and Roujean 2002) it is most likely that the pixels representing them are saturated. Hence the saturation and TM5 mask were combined resulting in a saturation mask that had no clouds. After that it was added to the NDSI mask and the water mask removed misidentified water areas.

At the final stage of computation a contiguity analysis was performed. Contiguous groups of pixels belonging to the same class, in this case Boolean 1, were identified by performing a clumping operation. Clumps were recoded to separate classes. It was decided that only the 4 orthogonal neighbours are considered contiguous. This prohibited the creation of elongated diagonal glacier clumps with only a width of ±30 m (Fig. 4).

A sieving procedure was applied to the clumped raster layers. After the clumping procedure the model produces a lookup table containing the histogram of the clumped layer that can be used to filter out small clumps from a layer. A scalar threshold value in pixels specified the minimum clump size to retain. A practical minimal glacier size of 0.1 km^2 is often applied in regional surveys. Here the threshold value was set to 110 pixels based on the ground resolution of the (E)TM(+) sensor. Thereafter small clumps were automatically recoded to the value zero. The method of clumping and sieving has a great advantage. No 'new' glacier pixels are created based on the neighbourhood properties of pixels such as in a method as filtering. The output glacier masks have a radiometric resolution of 1 bit and contain 2 Boolean classes, 1 for glacier and 0 for non-glacier.

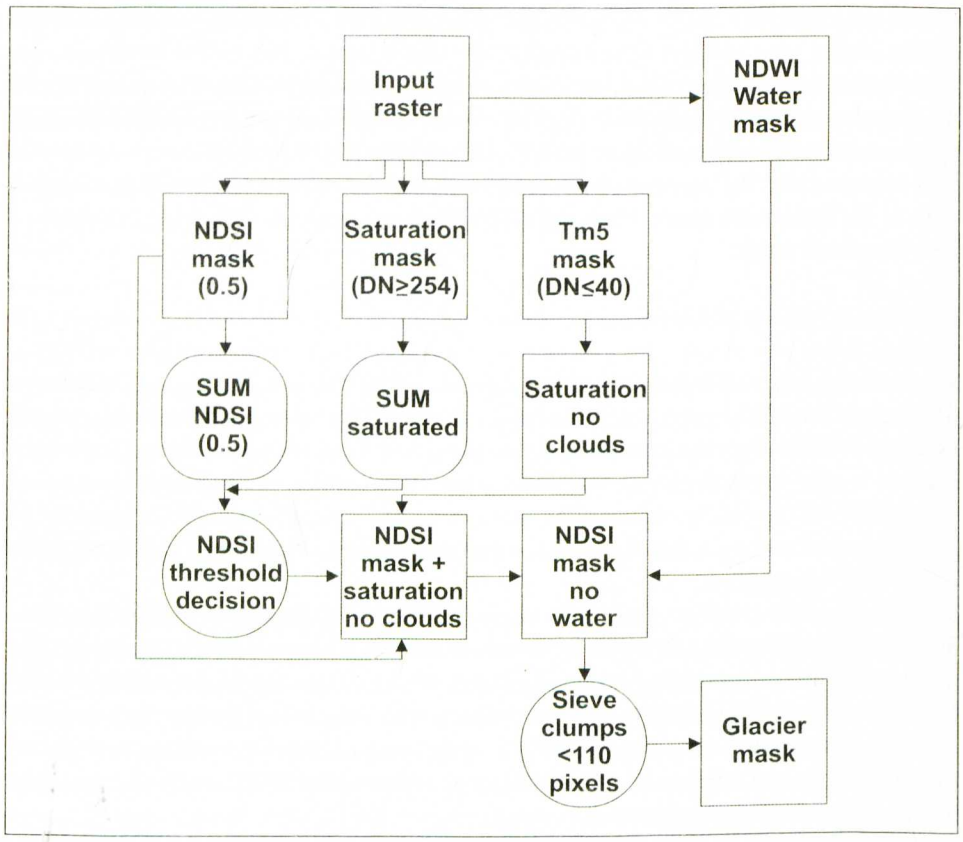

Figure 3. Schematic overview of the glacier masking procedure and decision criteria.

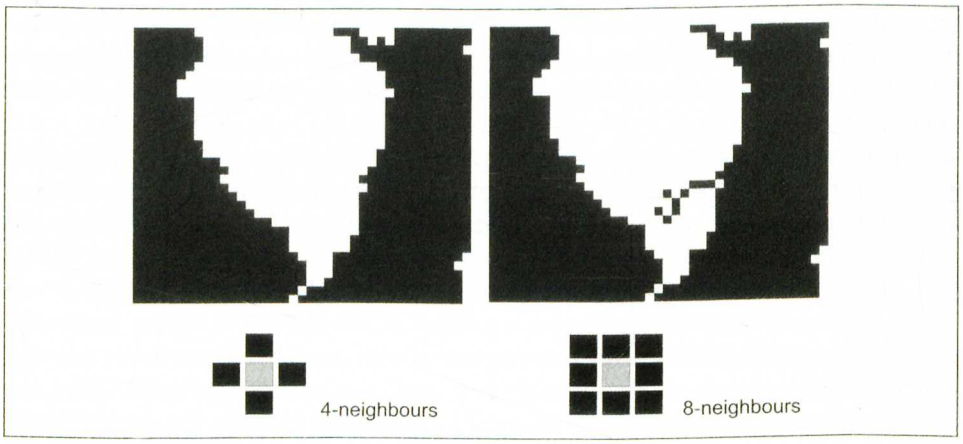

Figure 4. Illustration of clumping with 4 and 8 contiguous neighbours. Diagonally elongated features are created using 8 neighbours. Dark grey colours indicate the glacier area.

3.3 Accuracy and change analyses

As can be seen from Table 1, for the years 1991 and 1997 both Landsat TM images and grids from manually delineated glacier outlines were available, permitting accuracy analyses on the produced glacier masks for these years. The glacier outlines have been digitised onscreen based on visual interpretation of the accurate historical maps and glaciological knowledge of the glacier status for those years. The 1991 satellite image was orthorectified at the GLCF (Global Land Cover Facility, University of Maryland) and the registration error is not exactly known. Nevertheless, GLCF states that the overall positional accuracy for all produced images is just over 1 pixel (http://www.geocover.com). This is nearly the same accuracy when registering TM or ETM+ scenes perfectly to each other (Williams et al. 1997):

$$\text{Uncertainty} = (\text{Resolution}_{\text{image1}}{}^2 + \text{Resolution}_{\text{image2}}{}^2)^{1/2} \quad (5)$$

where the terms in the equation refer to the resolution of two images. The 1997 image was orthorectified using 143 GCPs (Ground Control Points) resulting in a general residual root mean square error (RMSE) of 0.7 pixels. The errors for measuring glacier termini when registering maps to satellite images are unknown (Hall et al. 2003). Visual comparison of the available grids and images of 1991 and 1997 revealed no inconsistencies in overlap at the edges of the glacier. Therefore the original rectifications were kept and they were not registered to each other.

The change analyses were carried out for the periods 1991–1997 and 1985–1999. The 1991–1997 period was validated by assessing the accuracy in terms of commissions and omissions when compared to the grids derived from the maps. Similarly, for the same period the accuracy of NDSI masks was assessed by comparing them to the grids derived from maps. The produced NDSI masks were therafter compared to the produced glacier masks in the modelling operation.

The area of Hintereisferner between 1894 and 2002 from grids and masks was put into a scatter plot to visualise the glacier retreat. Furthermore, a quantitative comparison of the area of Hintereisferner (1985–2002) was made between satellite-derived masks and terrestrial delineation. Visual change analyses for the area of Hintereisferner and neighbouring glaciers were carried out for the periods 1991–1997 and 1985–1999.

4. Results

4.1 Operation of the model

A visual representation of the results of the model for year 1997 is given in Figure 5. In the input-satellite image (Figure 5a), snow-covered glacier areas are white and ice areas are light grey. Water and cast shadows appear black. The input water masks are

not presented here but the threshold values used are tabulated further on in this paper in table 3.

The NDWI threshold values were found easily and e.g. the lake Gepatsch Stausee (Fig. 1) was delineated after 3 attempts for each of the 7 images. Retaining a saturation threshold value of ≥ 254 in band 1 demonstrates the high sensor saturation that may occur over glacierized areas (Fig. 5b). After applying the threshold of DN ≤ 40 to band 5 a TM5 mask was created. It shows in Figure 5c, that mainly water areas, glaciers and shadows were considered by the threshold to be non-cloud. The saturation mask and TM5 mask form the input of the mask shown in Figure 5d. It represents in black only those saturated pixels that are devoid from potential clouds. These pixels were assumed to be glacier. The initial and recalculated NDSI masks are shown in Figure 5e and 5f respectively. It can be seen that the Gepatsch Stausee is included in both masks. The initial mask includes larger areas identified as glacier as it was constructed using a lower NDSI threshold value. Figure 5g denotes the individual clumps after the spatial identification of contiguous groups of pixels. The grey scales mark the separate classes to which the clumps were recoded. Subsequently the resultant glacier mask is shown in Figure 5h. It excludes of clumps ≤ 0.1 km^2. The resulted glacier masking model procedure of first retrieving a water mask, entering inputs and outputs and running the model took less than half an hour.

4.2 Accuracy analyses

An accuracy analysis was carried out on the 1991 and 1997 glacier masks. As can be seen from Table 2 more than 80% of all pixels were identified correctly as glacier. In the table the accuracy is assessed for the quantitative match between the output glacier masks and reference grids. A criteria function was used to perform the analyses in which pixels present in both the reference grid and mask were assigned a value of 1, pixels not present in one of the masks were assigned a value of 2 or 3. The amounts of pixels correctly identified as glacier, omitted (not identified, but should have been) and committed (identified, but should not have been) are visualised in Figure 6. The largest contributions to error are the omissions at the tongue and margins of Hintereisferner. From Table 2 it becomes clear that about 13 to 17% ofthe glacier area is omitted This is not surprising as debris-covered and dirty ice is difficult to discriminate spectrally from scree on nearby slopes. Paul (1995) stated that when using thresholding methods sometimes the need of manual addition of debris covered areas can be as high as 20% of the glacier area. In Figure 6 the error bars represent the mean omission (15%) based on the accuracy analyses in Table 2.

It was observed that the smaller ice area located on the north-facing slope of the ridge Rofenköpfe had not been digitised in the reference grids. Therefore an effort was made to omit these pixels and re-assess the accuracy. Excluding 21 and 122 pixels from the 1991 and 1997 masks respectively resulted in slightly lower commissions but it

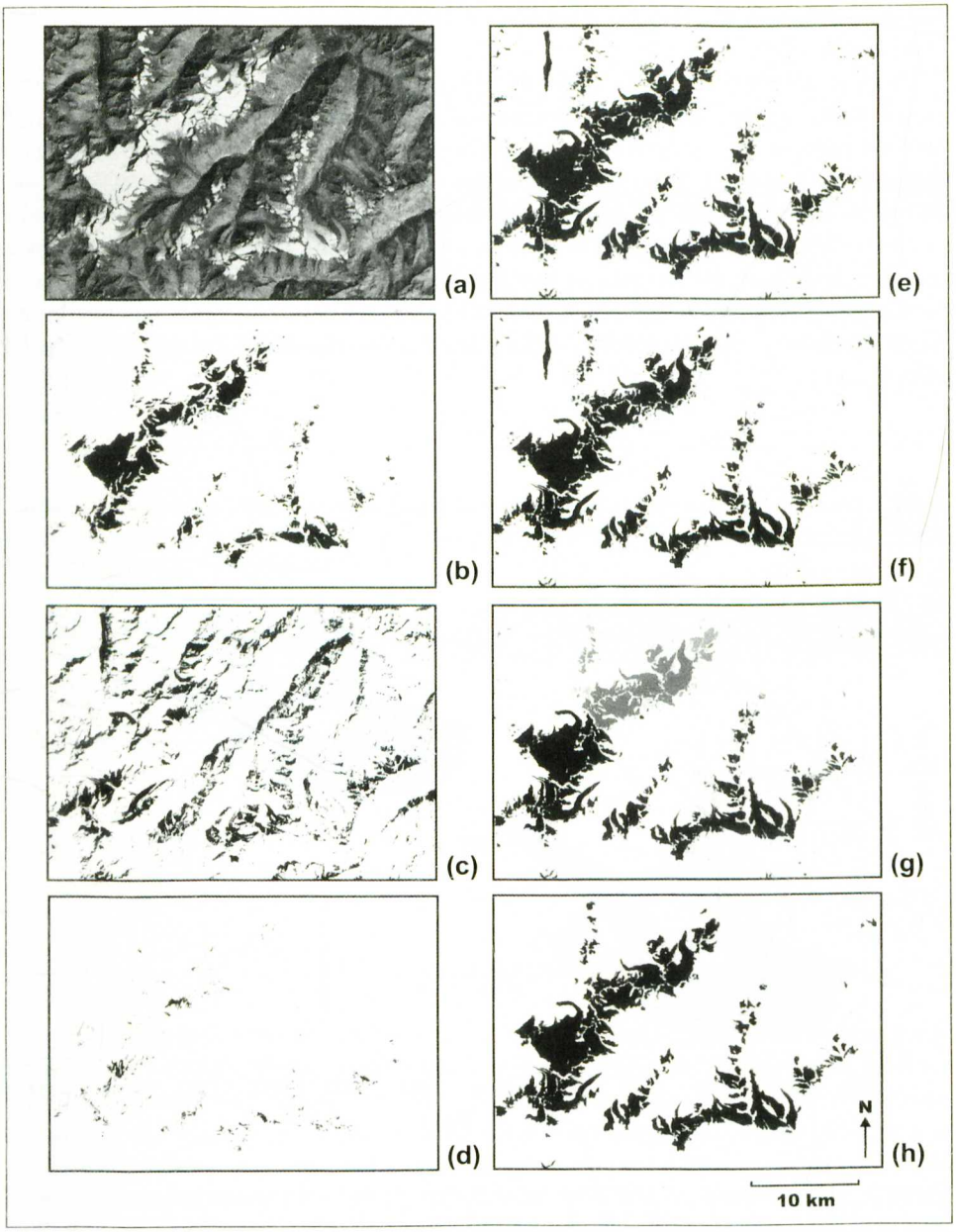

Figure 5. Overview of model output of the 1997 image. (a) Satellite image acquired on 15.09.1997, (b) saturation mask constructed from DN values ≥ 254 in TM1, (c) TM5 mask based on DN values ≤ 40, (d) saturated pixels present in the saturation mask but not in the TM5 mask, (e) NDSI mask created with initial threshold value 0.5, (f) recalculated NDSI mask plus the mask derived in (d), (g) clumped glacier mask, (h) glacier mask after sieving clumps of 110 pixels (~0.1 km^2).

had little effect on the amount of relative omission. Arrows in Figure 6 indicate these pixels in question.

Additionally the reference grids for Hintereisferner were compared to the individual NDSI masks, which are an intermediate result of the model. The computed NDSI threshold values from Equation 4 for years 1991 and 1997 are 0.59 and 0.60 respectively (Table 3). The results are in the same order of magnitude as when comparing the computed glacier masks to the reference grids. Even though the difference in correctly identified pixels in both masks is negligible, the NDSI mask will produce a worse result for the area of Hintereisferner and neighbouring glaciers. It is to be suspected that misclassification of water, dark shadows and snow patches in the NDSI mask (e.g. Fig. 5f) would produce large commissions of the extent of glacial areas.

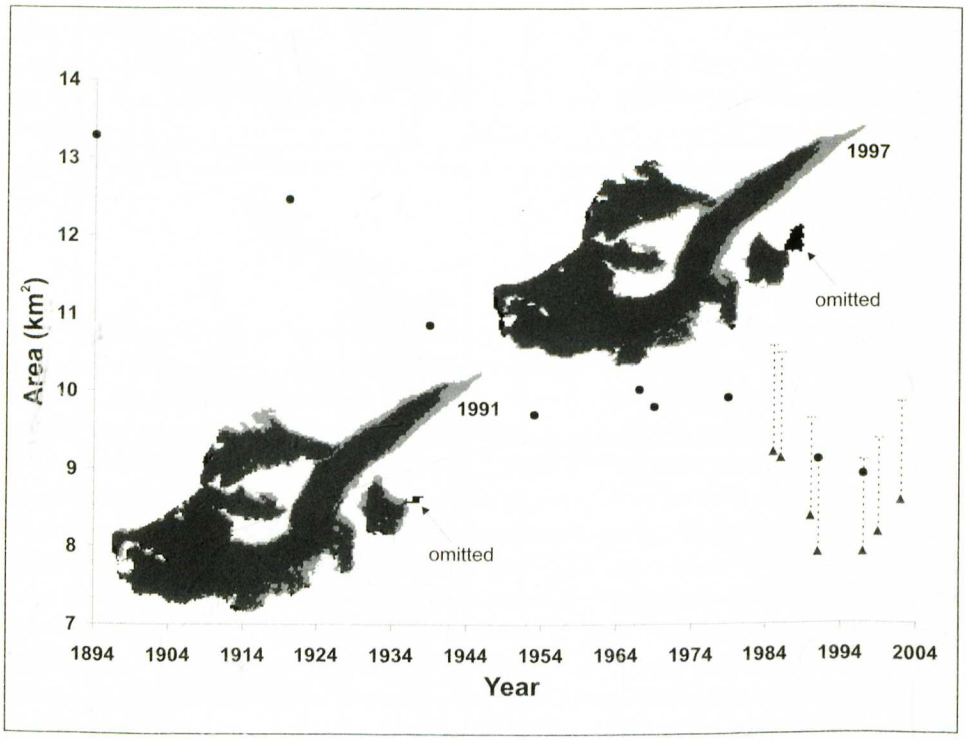

Figure 6. Change analyses of Hintereisferner for the 1991 and 1997 images and a scatter plot of the area of Hintereisferner 1894–2002. Dark grey colours in the images indicate correctly identifed pixels, light grey and black colours refer to omissions and commissions respectively. Omissions refer to those pixels that are classified as glacier but are not in real-time. Circles in the scatter plot are computed areas from reference grids, triangles are derived from the glacier masks (satellite). The error bars average 15% omissions. Arrows indicate omissions of the ice areas on the flanks of Rofenköpfe.

Table 2. Results of the accuracy analyses carried out for the years 1991 and 1997. The accuracy is shown as absolute (pixels) and relative (%) values. Omission stands for that amount of pixels that should have been classified correctly as glacier area according to comparison to grids. Commission are those pixels that are classified as glacier in de model output but are not classified as glacier in the produced grids.

	Comparison to grids		Comparison grid to NDSI	
Accuracy	1991 Pixels (%)	1997 Pixels (%)	1991 Pixels (%)	1997 Pixels (%)
Correct	8561 (80.92)	8548 (84.68)	8602 (80.56)	8584 (84.84)
Omission	1829 (17.29)	1297 (12.85)	1788 (16.74)	1261 (12.46)
Commission	189 (1.79)	250 (2.47)	288 (2.70)	273 (2.70)
Total	10579	10095	10678	10118

Table 3. Semi-automatically calculated NDSI threshold values. The lower NDWI threshold values utilised to create the water masks are given both as an absolute value and as an upper range (%) of DN value counts in the NDWI histogram.

Year	NDSI threshold	NDWI threshold (absolute / %)
1985	0.55	0.48 / 20
1986	0.54	0.45 / 20
1990	0.64	0.34 / 28
1991	0.59	0.40 / 23
1997	0.60	0.54 / 21
1999	0.55	0.45 / 20
2002	0.60	0.38 / 20

4.3 Area change analyses

From Table 4 it becomes clear that the model both omits and commits with a maximum omission of –10.8%. Unfortunately the largest omissions are for the years used for validation. During this period 1991–1997 practically no change in area is recorded by comparing the glaciers masks, but glaciological work reveals a decrease of 0.18 km^2 (Kuhn et al. 1999). The area of Hintereisferner decreased 1.17 km^2 between 1985 and 2002 according to Table 4 The change between the glacier masks for these years yields a decrease of only 0.62 km^2. The difference of 0.55 km^2 between these outcomes is most likely caused by the fairly high commission (+0.68 km^2) in 2002. The Landsat scene of 2002 contains some haze and has an intermediate NDSI threshold. Therefore, it is not entirely clear why the masking procedure commits. When comparing the change between 1985 and 1999, the difference between the two methods is only 0.19 km^2.

Table 4. Comparison of the area of Hintereisferner derived from glacier masks and data given by the Institute of Meteorology and Geophysics, University of Innsbruck.

Data from glaciological records		Data from images	
Glaciological Year	Area (km^2)	Year	Area (km^2) / difference from glaciological records (%)
1984–1985	9.07	1985	9.20 / +1.4
1985–1986	9.06	1986	9.12 / +0.7
1989–1990	8.88	1990	8.38 / –5.7
1990–1991	8.88	1991	7.92 / –10.8
1996–1997	8.70	1997	7.92 / –9.0
1998–1999	8.22	1999	8.16 / –0.7
2001–2002	7.90	2002	8.58 / +8.7

Areal changes for Hintereisferner and neighbouring glaciers as shown in the inset of Figure 2 were computed for 1991–1997 and 1985–1999. No validation could be performed as validation data for this larger area was absent except for 1997. The analysed area is about 720 km^2, computed glacier masks show that 159 km^2 and 138 km^2 of this area in 1985 and 1999 respectively were covered by glaciers. From 1985 to 1999 the whole area suffered a loss of nearly 25 km^2 while a gain of only 3.8 km^2 was found. The continuous negative mean annual specific balance during this period supports this observation (Kuhn et al. 1999).

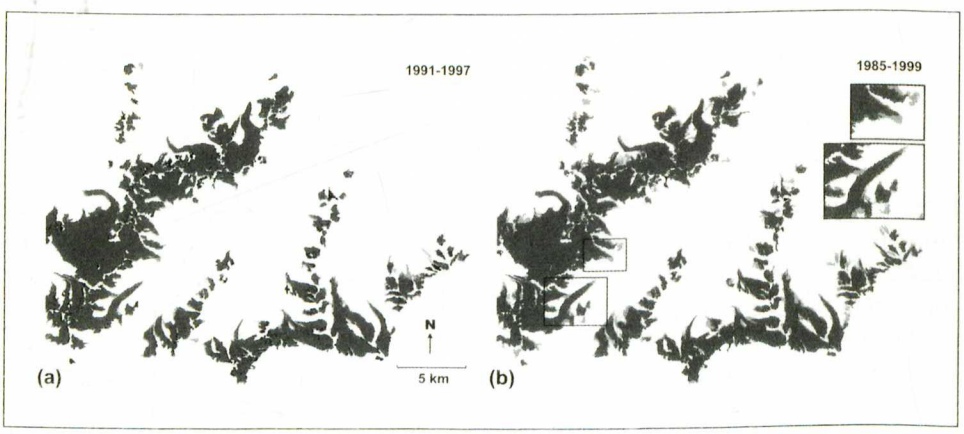

Figure 7. Change analyses of Hintereisferner and surroundings. (a) 1991–1997, (b) 1985–1999. Dark grey colours indicate no change, light grey and black are loss and gain in area respectively. The disconnection of Langtauferer-Joch-Ferner from Hintereisferner is shown in the larger inset. The retreat of the snout of Kesselwandferner is shown in the smaller inset.

Between 1991 and 1997 a gain in area of 6 km² was recorded. The 1991 mask of Hintereisferner and neighbouring glaciers contained multiple gaps of 1–4 pixels each, despite of the fairly high NDSI threshold used (0.59). Whilst comparing to the situation in 1997 these gaps produce the gain in area. Although finding the reason, it was decided not to manipulate the mask as the least possible manual alterations were desired. The changes in area are shown in Figure 7. It can be seen that the majority of calculated losses in area are at the tongues of individual glaciers and are consistent with the common retreat dynamics of glaciers. It is interesting to notice the retreat of the snout of the glacier Kesselwandferner (Inset Fig. 7b). Firstly it advanced 320 m between 1965–1985. Thereafter it started its retreat to the position in 1998 that corresponds to the one in 1965 (Span 1999). This retreat is shown in the inset of Figure 7b. It can be seen as well in the smaller inset that Langtauferer-Joch-Ferner lost its connection with Hintereisferner between 1985 and 1999.

5. Discussion

It was shown here that recognising glacier surfaces from space is well possible but might result in omissions close to the glacier's margins. Furthermore, the method presented here is a highly automated one for which the quality of area calculations and glacier outline could be assessed. It has been acknowledged earlier that the tongues of glaciers in recession are especially difficult to locate from satellite images (Williams et al. 1997). Debris on the surface impedes the spectral separation of the glacier area and scree on nearby slopes. Silverio and Jaquet (2005) separated the classes *glaciers* and *debris-covered glaciers* using both positive and negative NDSI criteria for each spectral classification theme. They assessed the accuracy using the formula for determining glacier tongue changes in flow direction given by Williams et al. (1997). The formula utilises the 30-m resolution of TM or ETM+ data and the registration error to a "base" satellite image. Their result of an uncertainty of ±10 % in area comes near the values found for omitting the area of Hintereisferner in 1997 (Table 2). When only looking at the accuracy of area calculations from the glacier masks (Table 4), the procedure presented here produced inaccuracies of less than 10 % except for 1990–1991. This is most probably caused by the one-month difference between the acquisition of the 1991-image (30.08) and the end of the glaciological year 1990–1991. Hall et al. (2003) acknowledged that after manual delineation of the glacier tongue of the Pasterze glacier in Austria it contained an area of 25 % covered by debris. This percentage is nearly double the amount of the omissions in the glacier masks for 1991 and 1997 (Table 2). Therefore it can be concluded that the automatic masking procedure without manual alterations works satisfactorily. The procedure is considered to work even better in advancing glaciers or on ice caps, like Svartisen, in which there is much less debris on the glacier surface than would be typical for retreating alpine valley glaciers, like Hintereisferner and most of the glaciers in the Alps in general (Koelemeijer et al.

1993). In future work, the method developed here will be tested for various glacier types and an assessment will be made to categorize the method in terms of limiting illumination conditions and latitudinal positions.

The area of Hintereisferner and neighbouring glaciers could not be validated due to the lack of reference data. Nevertheless, a clear retreat near the margins and termini of individual glaciers is visible for the period 1985–1999 (Fig. 7) and consistent with glacier dynamics. Most of the retreat occurs near the margins and termini of individual glaciers.

As it was assumed that the reference grids are the most accurate datasets available for validation, the masking procedure performs well within the limits of inaccuracy set in other studies. Although the simple NDSI thresholding procedure performs a little better in identifying pixels correctly for Hintereisferner, the result will be worse over the area of Hintereisferner and neighbouring glaciers. The NDSI includes water bodies when an optimal NDSI threshold for detecting the glacier area is found. These areas would have to be removed manually. Alternatively Sidjak and Wheate (1999) experimented with combinations of NDSI, band rationing TM bands 4 / 5 and principal component analyses for glacier mapping. After numerous attempts to filter out shadows they produced a fairly good glacier mask. Compared to these combinations or a NDSI masking procedure, the current semi-automatic method using (E)TM(+)5 and saturated pixels as a cloud filter proves to be fast, sufficiently accurate and devoid of major anomalies. For monitoring purposes, this allows a fast interpretation of multitemporal glacier outlines. Most probably the quality of the masks would improve when information on the thermal properties of the glacier area is incorporated in the thresholding procedure (Hendriks and Pellikka 2004). This would allow the separation of debris-covered glacier surfaces and their surroundings. Images were used here from Landsat missions 4–7. Unfortunately the resolutions of the thermal-infrared bands differ from 60 m to 120 m for TM and ETM+ respectively. This makes the accuracy assessment even more troublesome when creating masks from 30-m pixels. Furthermore, thermal bands tend to have a high degree of unevenness or 'striping' throughout the scene. This is a result only of ground processing and at present it is only corrected for the latest ETM+ data starting from 1999 (http://landsat.usgs.gov/). An implementation of separate thresholds for glaciers and debris-covered glaciers (Silverio and Jaquet 2005) most probably will not resolve certain inaccuracies (like ommissions) for large glacier areas. The range in DN values will be too substantial to avoid the exclusion of numerous non-glacier pixels that lie within the threshold ranges.

6. Conclusions

Semi-automatic glacier delineation of Hintereisferner from Landsat imagery using a set of conditional operators on spectral bands works satisfactory within known error limits. Produced glacier masks were compared to reference grids derived from digitised maps. For the years 1991 and 1997 both satellite images and reference grids were available and the accuracy of the masking procedure was assessed to be more than 80% of for both years. The largest sources of error were the omissions. The areas that were omitted are located at the tongue and margins of the glacier. This can be attributed to the debris contributed from slopes. It covered the lower parts of the glacier and could not be discriminated spectrally from scree on slopes. Despite the development of new remote sensing techniques, only traditional glaciological field investigations by experts can unveil debris-covered areas belonging to the glacier.

7. Acknowledgements

This work was funded by the OMEGA Project (European Commission 5th Framework Programme: Environment and Sustainable Development, Development of generic Earth observation technologies; Contract No. EVK2-CT-2000-00069). We would like to thank our colleagues in the Ice and Climate Group at the Institute for Meteorology and Geophysics, University of Innsbruck, Austria for all their help and supplying the reference data.

8. References

Bayr, K. J., D. K. Hall, and W. M. Kovalick, 1994: Observations on glaciers in the eastern Austrian Alps using satellite data. *International Journal of Remote Sensing* 15, 1733–1742.

Blümcke, A., and H. Hess, 1899: Untersuchungen am Hintereisferner. *Wissenschaftliche Ergänzungshefte zur Zeitschrift des Deutschen und Österreichischen Alpenvereins* 1 (2), München: Bruckmann AG, 1–87.

Choi, H., and R. Bindschadler, 2004: Cloud detection in Landsat imagery of ice sheets using shadow matching technique and automatic normalized difference snow index threshold value decision. *Remote Sensing of Environment* 91, 237–242.

Della Ventura, A., A. Rampini, R. Rabagliati, and R. Serandrei Barbero, 1983: Glacier monitoring by satellite. *Il Nuovo Cimento* C–1 (6), 211–221.

Gratton, D. J., P. J. Howarth, and D. J. Marceau, 1990: Combining DEM parameters with Landsat MSS and TM imagery in a GIS for mountain glacier characterization. *IEEE Transactions on Geoscience and Remote Sensing* GE–28, 766–769.

Hall, D. K., A. T. C. Chang, and H. Siddalingaiah, 1988: Reflectances of glaciers as calculated using Landsat 5 Thematic Mapper data. *Remote Sensing of Environment* 25, 311–321.

Hall, D. K., G. A. Riggs, and V. V. Salomonson, 1995: Development of methods for mapping global snow cover using Moderate Resolution Imaging Spectroradiometer (MODIS) data. *Remote Sensing of Environment* 54, 127–140.

Hall, D. K., K. J. Bayr, W. Schöner, R. A. Bindschadler, and J. Y. L. Chien, 2003: Consideration of the errors inherent in mapping historical glacier positions in Austria from the ground and space (1893–2001). *Remote Sensing of Environment* 86, 566–577.

Heiskanen, J., 2003: *Assessment of glacier changes and mass balance using Landsat satellite data in Svartisen, Northern Norway*. Department of Geography, University of Turku, Finland. Master Thesis (in Finnish), 149 p.

Heiskanen, J., K. Kajuutti, M. Jackson, H. Elvehøy, and P. Pellikka, 2003: Assessment of glaciological parameters using Landsat satellite data in Svartisen, Northern Norway. *EARSeL eProceedings* 2 1/2003, 34–42. Observing our Cryosphere from Space.

Hendriks, J. P. M., and P. Pellikka, 2004: Estimation of reflectance from a glacier surface by comparing spectrometer measurements with satellite-derived reflectances. *Zeitschrift für Gletscherkunde und Glazialgeologie* 38 (2), 139–154.

Hoinkes, H., 1970: Methoden und Möglichkeiten von Massenhaushaltsstudien auf Gletschern, Ergebnisse der Messreihe Hintereisferner (Ötztaler Alpen) 1953–1968. *Zeitschrift für Gletscherkunde und Glazialgeologie* 6, 37–90.

Kääb, A., F. Paul, M. Maisch, M. Hoelzle, and W. Haeberli, 2002: The new remote-sensing-derived Swiss glacier inventory: II. First results. *Annals of Glaciology* 34, 362–366.

Koelemeijer, R., J. Oerlemans, and S. Tjemkes, 1993: Surface reflectance of Hintereisferner, Austria, from Landsat 5 TM imagery. *Annals of Glaciology* 17, 17–22.

Kuhn, M., N. Span, and H. Schneider, 1996: Changing Mode of Ice Flow During Advances of Hintereisferner. *CRREL Special Report*, Cold Regions Research and Engineering Laboratory, Hanover, NH., 96 (27), 69–74.

Kuhn, M., E. Schlosser, and N. Span, 1997: Eastern Alpine glacier activity and climatic records since 1860. *Annals of Glaciology* 24, 164–168.

Kuhn, M., E. Dreiseitl, S. Hofinger, G. Markl, N. Span, and G. Kaser, 1999: Measurements and models of the mass balance of Hintereisferner. *Geografiska Annaler* 81 A (4), 659–670.

Lambrecht, A., and M. Kuhn, 2007: Glacier changes in the Austrian Alps during the last three decades, derived from the new Austrian Glacier Inventory. *Annals of Glaciology* 46, 177–184.

van Leeuwen, W. J. D., and J.-L. Roujean, 2002: Land surface albedo from the synergistic use of polar (EPS) and geo-stationary (MSG) observing systems. An assessment of physical uncertainties. *Remote Sensing of Environment* 81, 273–289.

McFeeters S. K., 1996: The use of the Normalized Difference Water Index (NDWI) in the delineation of open water features. *International Journal of Remote Sensing* 17 (7), 1425–1432.

Østrem, G., 1975: ERTS-1 data in glaciology – an effort to monitor glacier mass balance from satellite imagery. *Journal of Glaciology* 15, 403–415.

Paul, F., 2002: Changes in glacier area in Tyrol, Austria, between 1969 and 1992 derived from Landsat 5 Thematic Mapper and Austrian Glacier Inventory Data. *International Journal of Remote Sensing* 23 (4), 787–799.

Paul, F., C. Huggel, and A. Kääb, 2004: Combining satellite multispectral image data and a digital elevation model for mapping debris-covered glaciers. *Remote Sensing of Environment* 89, 510–518.

Rott, H., and G. Markl, 1989: Improved Snow and Glacier Monitoring by the Landsat Thematic Mapper. *Proceedings of a Workshop on 'Earthnet Pilot Project on Landsat Thematic Mapper Applications'*, Frascati, Italy, 10 p.

Rott, H., 1976: Analyse der Schneeflächen auf Gletschern der Tiroler Zentralalpen aus Landsat Bildern, *Zeitschrift für Gletscherkunde und Glazialgeologie* 12 (1), 1–28.

Schlosser, E., 1996: Numerical simulation of fluctuations of Hintereisferner, Ötztal Alps, back to 1850 A. D. *Zeitschrift für Gletscherkunde und Glazialgeologie* 32, 151–152.

Sidjak, R. W., and R. D. Wheate, 1999: Glacier mapping of the Illecillewaet icefield, British Columbia, Canada, using Landsat TM and digital elevation data. *International Journal of Remote Sensing* 20, 273–284.

Silverio, W., and J. M. Jaquet, 2005: Glacial cover mapping (1987–1996) of the Cordillera Blanca (Peru) using satellite imagery. *Remote Sensing of Environment* 95, 342–350.

Span, N., 1993: *Untersuchung der Dynamik des Hintereisferners zwischen 1894 u. 1992*. Master thesis (in German), University of Innsbruck, 111 p.

Span N., 1999: *Zur Dynamik des Kesselwandferners*. Dissertation (in German), University of Innsbruck, 214 p.

Span, N., M. Kuhn, and H. Schneider, 1997: 100 years of ice dynamics of Hintereisferner, Central Alps, Austria, 1894–1994. *Annals of Glaciology* 24, 297–302.

Williams, R. S. Jr., D. K. Hall, O. Sigurdsson, and J. Y. L. Chien, 1997: Comparison of satellite-derived with ground-based measurements of the fluctuations of the margins of Vatnajökull, Iceland, 1973–92. *Annals of Glaciology* 24, 72–80.

Würländer R., and M. Kuhn, 2000: Zur Erstellung und Anwendung der Produkte des neuen Österreichischen Gletscherkatasters. *Salzburger Geographische Arbeiten* 36, 57–67.

http://landsat.gsfc.nasa.gov/project/Comparison.html (Visited on 11.03.2005).

http://www.geocover.com (Visited on 15.03.2005).

Manuscript received 12.4.2005, revised 13.11.2007.

Authors' address: Johan P. M. Hendriks
Johan.Hendriks@helsinki.fi

Petri Pellikka
University of Helsinki, Department of Geography
P. O. Box 64 (Gustaf Hällströmin katu 2)
FIN–00014 Helsinki, Finland